BHAM-HEP/96-06
17 December 1996

ELECTROWEAK RESULTS FROM LEP[1]

D.G. CHARLTON

[a] *Royal Society University Research Fellow, School of Physics and Space Research, University of Birmingham, Birmingham B15 2TT, UK*

Abstract

The status of electroweak measurements at LEP is reviewed. Good agreement with the Standard Model predictions is observed. Previous reports of possible deviations from the Standard Model expectations of the partial widths for Z^0 decays to heavy quarks have become less significant with the addition of more data. In the forthcoming LEP-2 phase, the focus of electroweak measurements at LEP will switch to a precise measurement of the W mass.

1 Introduction

The precision of electroweak measurements at the Z^0 at LEP is now very high, exceeding the original anticipations[1]. In particular, high precision energy scans around the Z^0 have allowed the Z width to be measured with a fractional precision of 0.13%, and the Z mass to 2.4×10^{-5}. Overall, the measurements provide an impressive confirmation of the electroweak theory. Measurements in the heavy quark sector are also now of sufficient precision to probe the structure of the theory, being sensitive to possible loop effects beyond the Standard Model.

The year of 1996 sees a transition in the mode of operation of LEP, as the beam energy is increased from the region of the Z^0 resonance ("LEP-1" data-taking), to the W pair production threshold and beyond ("LEP-2"). The first physics results from e^+e^- collisions well above the Z^0 have been obtained from a first short pilot run ("LEP-1.5") at 130-140 GeV centre-of-mass energy in autumn 1995.

The structure of this report is as follows: first the Z^0 lineshape and asymmetry results are summarised. Next, heavy flavour electroweak measurements are discussed, in more detail, before a review of the implications of the full set of electroweak results in the Standard Model framework. Finally, the future of electroweak physics at LEP is surveyed briefly.

2 The Z^0 Lineshape

The cross-section for e^+e^- annihilation into hadrons, corrected to the Born level, is shown in figure 1. The three characteristic Z^0 lineshape parameters within the Standard Model, the Z^0 mass, M_Z, the width, Γ_Z, and the pole cross-section, $\sigma^{\rm pole}_{\rm had}$, are indicated. The cross-section for e^+e^- annihilation into hadrons is measured at a few centre-of-mass energy points across the Z^0 resonance, and M_Z, Γ_Z and $\sigma^{\rm pole}_{\rm had}$ are extracted by fitting the expected resonance shape as a function of these parameters.

It was decided to perform an energy scan of LEP around the Z^0 during the last year of LEP-1 operation, in 1995, primarily in order to improve the statistical precision on the Z^0 width, Γ_Z. The measurement of $\sigma^{\rm pole}_{\rm had}$ was possible using the high statistics on-peak Z^0 data from the 1994 run, and the result is dominated by a theoretical uncertainty on the Bhabha scattering cross-section used to

[1]Invited talk presented at the 20th Johns Hopkins Workshop on Non-Perturbative Particle Theory and Experimental Tests, Heidelberg, Germany, 27-29 June 1996.

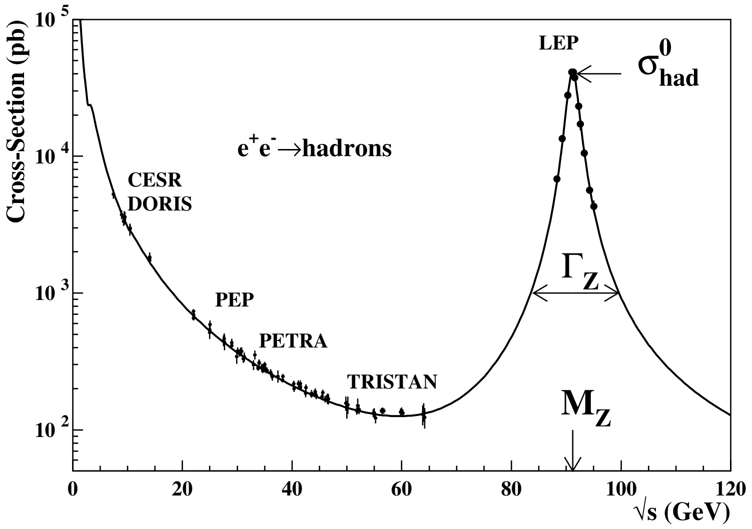

Figure 1: Measured and expected e^+e^- annihilation cross-section into hadronic final states, corrected to the Born level.

measure luminosity, common between the LEP experiments. It was expected that the measurement of M_Z would also be improved by the scan, but less than Γ_Z since the systematic error on M_Z from the LEP beam energy was relatively large.

The scan was carried out successfully during the year, and effectively doubled the available data sample from centre-of-mass energies at the sides of the Z^0 peak. The analyses of these 1995 data are still in progress[2]. The high statistical precision of these data requires care and close attention to possible experimental systematic errors. One area of which the understanding was significantly improved as a result of the energy scan was the issue of the energy calibration of the LEP machine, which is critically important for the M_Z and Γ_Z measurements.

2.1 LEP Energy Calibration

Extensive studies of the energy calibration of LEP were made for the 1993 energy scan[3]. The technique of resonant depolarisation of the circulating electrons leads to a measurement of the average energy in the LEP ring with a precision of better than 1 MeV at the time of measurement. However, the energy calibration measurements were only made in a minority of off-peak physics coasts ("fills"), and almost always at the ends of those fills. A special model was constructed to imitate different effects which can change the beam energy, such as tides, temperature variations, and so on. The energy model can then be used to extrapolate to all fills from those measured by resonant depolarisation. The energy extrapolation resulted in an uncertainty which increased the estimated energy error to a few MeV.

The position was markedly improved in the 1995 scan[4] by performing a resonant depolarisation measurement in approximately two-thirds of the off-peak LEP fills. The sophistication of the energy model was also improved. Using the model to predict the energies at the depolarisation calibration time, residual scatters at the level of just 3 MeV were found. Various new checks of the energy variations were also made, for example by occasionally also measuring the energy at the start of fill, and by monitoring the bending fields during a fill using nuclear magnetic resonance (NMR) probes.

[2] The first preliminary results were shown at the July/August 1996 conferences[2], but were not available for this workshop. Electroweak results from these summer conferences are indicated in footnotes in this writeup, where they are relevant to the discussion.

The checks using the NMR probes installed inside the bending magnets however revealed a completely unexpected behaviour during each physics coast, which was eventually found to be correlated with the passing of French electric TGV trains along the railway line near to CERN. The measurements of the bending field from the NMR probes are compared with the voltage observed on these nearby rail lines as a train passed in figure 2. The correlation is manifest. The origin of the problem

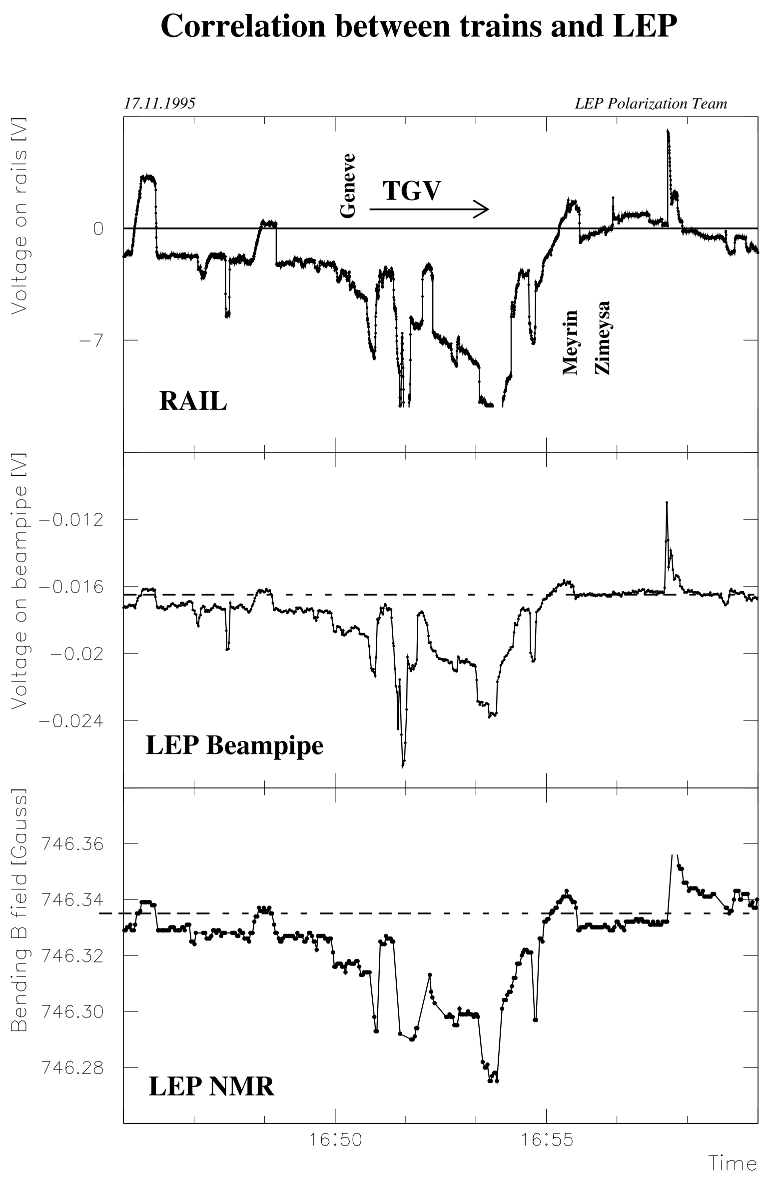

Figure 2: Variation of bending field observed in LEP magnets (bottom) compared to voltage observed on rail lines in local area (top) and voltage measured on the LEP beampipe (middle) as a function of time, as a train passes by.

is now understood to arise from a small return current passing along the LEP beampipe when a train passes (see figure 3). This transitory circulating current is sufficient to induce bending magnet field shifts from hysteresis effects. These lead in turn to beam energy shifts, which can be as large as several MeV accumulated over a whole fill.

The size of this effect is, however, expected to be similar at all energy points, since the choice of energy is uncorrelated with the time of day, and a large number of fills are made at each energy point during a scan. This means that the effect does not impinge significantly on the measurement of the Z

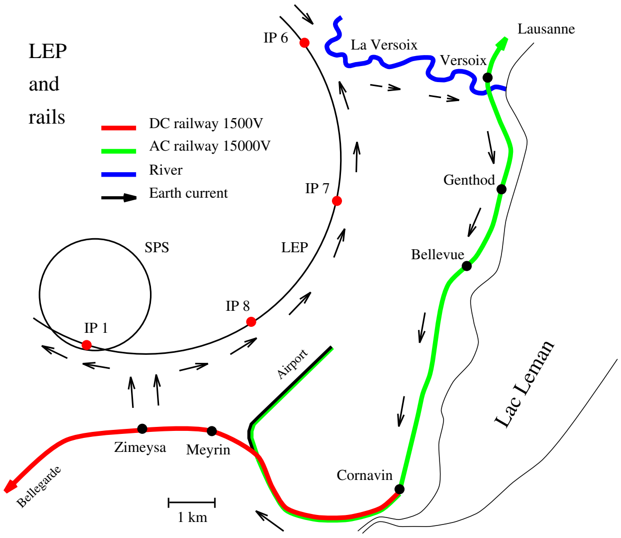

Figure 3: Schematic picture of the current flow postulated as a possible explanation of the "TGV effect".

width, as the relative energy scale is only very weakly affected. On the other hand, the value of the Z mass extracted from the data is directly affected by any mean energy shift during fills[3].

3 Asymmetries in Leptonic Z^0 Decays

The charged lepton couplings of the Z^0 can be probed both by measuring the cross-section for lepton pair production across the Z^0 peak, and from various asymmetry parameters. In the lepton sector, the charged lepton forward-backward asymmetries and the tau polarisation have been measured at LEP[5]. The left-right forward-backward asymmetry has also been measured in Z^0 decays, by SLD at SLAC[6].

In the Standard Model, the leptonic forward-backward asymmetry, defined as:

$$A^{\mathrm{f}}_{\mathrm{FB}} = \frac{\sigma_{\mathrm{F}} - \sigma_{\mathrm{B}}}{\sigma_{\mathrm{F}} + \sigma_{\mathrm{B}}},$$

can be expressed on the Z^0 pole in terms of the asymmetry parameters $\mathcal{A}_{\mathrm{f}}$:

$$A^{0,\mathrm{f}}_{\mathrm{FB}} \equiv \frac{3}{4}\mathcal{A}_{\mathrm{e}}\mathcal{A}_{\mathrm{f}}, \qquad \mathcal{A}_{\mathrm{f}} = 2\frac{v_{\mathrm{f}} a_{\mathrm{f}}}{(v_{\mathrm{f}}^2 + a_{\mathrm{f}}^2)}.$$

The asymmetry parameters are just a function of the ratio of vector to axial vector couplings of the Z^0 to that fermion species f:

$$\frac{v_{\mathrm{f}}}{a_{\mathrm{f}}} = (1 - 4|Q_{\mathrm{f}}|\sin^2\theta_{\mathrm{W}}^{\mathrm{eff,f}})$$

thus making the asymmetries sensitive to the effective electroweak mixing angle $\sin^2\theta_{\mathrm{W}}^{\mathrm{eff}}$.

The angular distribution of $e^+e^- \to \mu^+\mu^-$ scattering is illustrated in figure 4. The centre-of-mass energy dependence of the forward-backward asymmetry is also evident in this figure. This energy dependence originates from the changing relative sizes of the Z^0-exchange, the γ-exchange, and the Z^0-γ-interference contributions.

[3]The size of this effect has since been found[2] to give approximately a 4 MeV downward correction to M_{Z}.

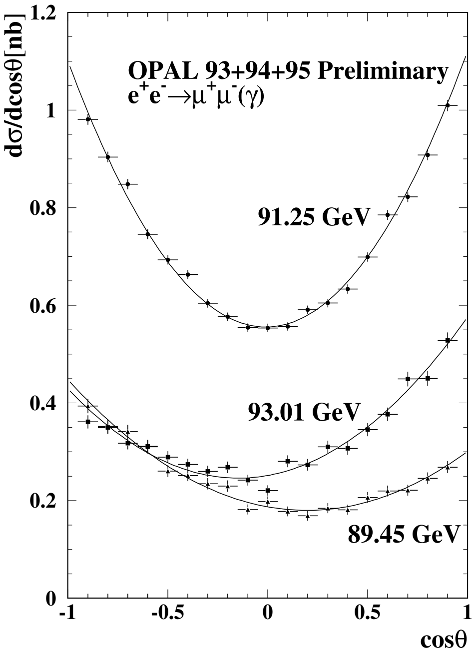

Figure 4: Measured cross-section for $e^+e^- \to \mu^+\mu^-$ at three centre-of-mass energies, as observed by OPAL.

The $\cos\theta$ dependence of the tau polarisation can also be used to measure the $\mathcal{A}_f$ parameters:

$$\mathcal{P}_\tau(\cos\theta) = -\frac{\mathcal{A}_\tau(1+\cos\theta^2) + \mathcal{A}_e 2\cos\theta}{(1+\cos\theta^2) + \mathcal{A}_\tau\mathcal{A}_e 2\cos\theta}$$

which allows both $\mathcal{A}_\tau$ and $\mathcal{A}_e$ to be extracted together. The combined LEP results obtained are:

$$\begin{aligned} \mathcal{A}_\tau &= 0.1394 \pm 0.0069 \\ \mathcal{A}_e &= 0.1429 \pm 0.0079\,, \end{aligned}$$

consistent with lepton universality.

4 Combined Z^0 Lineshape and Lepton Asymmetry Results

The hadron and lepton cross-sections measured across the Z^0 resonance, and the measured lepton forward-backward asymmetries, can be combined assuming the Standard Model framework. Technically, the results from the four LEP experiments are combined by making use of variables which are only minimally correlated experimentally:

- M_Z, Γ_Z, $\sigma^{\rm pole}_{\rm had}$, the Z^0 lineshape parameters
- $R_e \equiv \Gamma_{\rm had}/\Gamma_{ee}$, R_μ, R_τ, the ratios of the partial decay widths of the Z^0 to hadrons relative to that to leptons
- $A^{0,e}_{\rm FB}$, $A^{0,\mu}_{\rm FB}$, $A^{0,\tau}_{\rm FB}$ the pole lepton forward-backward asymmetries

The common systematic errors in the measurements between experiments, such as the LEP energy and luminosity theoretical uncertainties, are accounted for separately. The combination is made in two stages: first lepton universality is not assumed, and the average values of R_e, R_μ, R_τ, $A^{0,e}_{\rm FB}$, $A^{0,\mu}_{\rm FB}$ and $A^{0,\tau}_{\rm FB}$ are obtained; and secondly the combination is repeated assuming lepton universality. The first

Table 1: Lineshape and lepton asymmetry parameters from fits to the data of the four LEP experiments, assuming lepton universality[7]. The correlations between the different extracted parameters are small, being 15% or less.

	M_Z (MeV)	Γ_Z (MeV)	$\sigma^{\text{pole}}_{\text{had}}$ (nb)	R_ℓ	$A^{0,\ell}_{\text{FB}}$
ALEPH	91192.3±3.7	2495.2±5.5	41.56±0.09	20.738±0.060	0.0190±0.0020
DELPHI	91184.9±3.4	2491.7±5.3	41.40±0.10	20.704±0.073	0.0179±0.0023
L3	91193.8±3.6	2502.2±5.4	41.48±0.11	20.811±0.076	0.0186±0.0030
OPAL	91184.6±3.5	2495.9±5.3	41.47±0.10	20.851±0.059	0.0142±0.0020
LEP	91188.4±2.2	2496.4±3.2	41.490±0.078	20.789±0.032	0.0172±0.0012

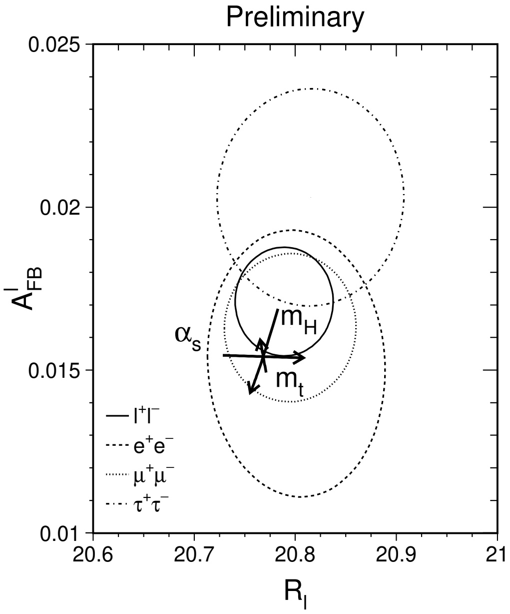

Figure 5: Test of lepton universality in Z^0 decays. The Standard Model prediction is shown by the arrows, which indicate the variations $m_{\text{top}} = 175 \pm 9$ GeV, $m_{\text{H}} = 300^{+700}_{-240}$ GeV and $\alpha_s(M_Z) = 0.123 \pm 0.006$. The curves are 68% C.L. contours.

combination is used to check lepton universality: the results are shown in figure 5. No incompatibility with the hypothesis of lepton universality is observed. The results of the second combination are given in table 1. These results include the 1990 to 1994 data.

The combined fits can also be used to check the invisible width of the Z^0 is consistent with expectation. The value:

$$\Gamma_{\text{inv}}/\Gamma_{\ell\ell} = 5.954 \pm 0.031$$

is obtained, where Γ_{inv} is the invisible width of the Z^0, found by subtracting the observed hadronic and charged lepton widths from Γ_Z. This can be converted to an effective number of light neutrino flavours, N_ν, using the Standard Model expectation for the ratio of the neutrino width to the charged leptonic partial width, $(\Gamma_\nu/\Gamma_{\ell\ell})_{\text{SM}} = 1.991 \pm 0.001$ to give:

$$N_\nu = 2.991 \pm 0.016$$

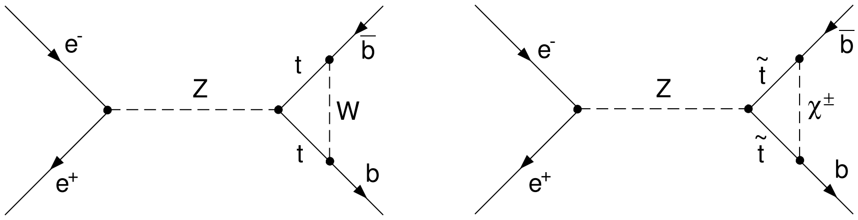

Figure 6: Diagrams which may give special corrections to the $Z^0 b\overline{b}$ vertex: on the left from a Standard Model diagram, on the right for a possible supersymmetric contribution.

5 Heavy Quark Measurements

Decays of the Z^0 to heavy quark pairs can be separated statistically from other hadronic Z^0 decays, using specially designed heavy flavour tags. From these enriched heavy quark samples both the Z^0 partial decay widths and forward-backward asymmetries can be measured[8], for b and c quark decays of the Z^0.

Experimentally, the ratio of partial widths of the Z^0 to $b\overline{b}$ or $c\overline{c}$ is measured from the ratio of cross-sections for $b\overline{b}$ and $c\overline{c}$ to hadronic event production. This latter ratio is known as "R_b" or "R_c" for b and c quarks, respectively:

$$R_Q = \frac{\sigma(e^+e^- \to Q\overline{Q})}{\sigma(e^+e^- \to \text{hadrons})} \simeq \frac{\Gamma(Z^0 \to Q\overline{Q})}{\Gamma(Z^0 \to \text{hadrons})}.$$

The inequality is only inexact because of the necessity for small corrections to take into account γ exchange, and γ-Z^0 interference. In addition to the experimentally accessible nature of the ratio R_Q, there is a further advantage that the Standard Model prediction of it does not have a very strong dependence on the details of many radiative corrections, particularly the propagator and initial-state QED corrections. These corrections are common to both the heavy quark and total hadronic widths, and so cancel in forming the ratio. Therefore R_Q measurements may be interpreted as a rather direct test of the couplings at the $Z^0 Q\overline{Q}$ vertex. In the case of R_b this may be particularly intriguing, as the $Z^0 b\overline{b}$ vertex is expected[9] to have special corrections both within the context of the Standard Model (from top loops), and also in many extensions to the Standard Model (see figure 6).

The techniques for measuring the partial widths R_c and R_b are discussed in the following two subsections. A brief overview is then given of the current heavy quark forward-backward asymmetry measurements. The different properties of c and b tags are central to the relative precisions of these measurements. As discussed below, c tags are mostly based on exclusive or semi-exclusive reconstruction of decaying charm hadrons, while b tags make use of much more inclusive lifetime tags, which have a much higher efficiency and a better purity. As a result, the precision of measurements of R_b is significantly better than that for R_c. In addition, leptonically decaying b and c hadrons can be tagged by identifying the produced lepton. These tags are particularly of note for asymmetry measurements, as the lepton charge allows the decaying heavy quark charge to be inferred directly. It is unfortunately not possible to cover these lepton tag measurements in any detail here.

5.1 Measurements of R_c

The measurements of R_c using exclusive and semi-exclusive charm hadron reconstruction can be subdivided into three classes. Several elements are common to these different methods of extracting R_c from a measurement of the yield of a specific c hadron decay:

- Reconstructed hadrons coming from c quarks produced in $Z^0 \to c\overline{c}$ decays must be separated from those from $Z^0 \to b\overline{b}$ decays, with subsequent $b \to c$ decay. These two sources of charm hadrons are of similar sizes. A variety of techniques for the statistical separation of the two components have been developed, but most separating power comes from the different lifetimes of b and c hadrons.

- In converting from the observed yield of a specific reconstructed decay channel to the actual number of such decays, the reconstruction efficiency of the detector has to be known. This is typically obtained from Monte Carlo detector simulation.

- In converting from the corrected number of specific hadron decays to the number of produced hadrons of that type, the decay branching ratio into the reconstructed channel must be known. These branching ratios are usually taken from lower energy measurements, although some new measurements from LEP are becoming available.

- Finally, in extracting the number of $Z^0 \to c\bar{c}$ events from the number of produced hadrons of a given type, after b/c flavour separation, it is still necessary to know the probability that a c quark produced in the Z^0 decay hadronises into that specific charmed hadron. These so-called "hadronisation fractions", $P_{c\to X}$, have to be taken as external inputs to some of the measurements.

All of these uncertainties can give rise to systematic errors on R_c from these reconstructed hadron analyses, and in some cases these uncertainties can be strongly correlated between the different measurements.

The oldest technique for measuring R_c relies upon measuring the yield of D^{*+} mesons. Converting this yield to R_c requires knowledge of all the quantities just described. To try to reduce the systematic error coming from these uncertainties a double-tag approach has been developed which allows the product $P_{c\to D^{*+}}B(D^{*+} \to D^0\pi^+)$ to be measured simultaneously from the LEP data. These new double-tag measurements constitute the second class of reconstructed hadron R_c measurements. The final, also quite novel, technique removes the hadronisation uncertainties in a different way, by instead reconstructing signals for decays of each of D^0,D^+,D_s^+ and Λ_c^+ hadrons. This allows the hadronisation fractions $P_{c\to X}$ to be measured simultaneously with R_c. The three techniques are described in more detail in the following.

The single-tag measurement of R_c from the D^{*+} production rate uses the special kinematics of the decay $D^{*+} \to \pi^+D^0$, which is just above threshold. As a result, the distribution of the mass difference $M_{D^{*+}} - M_{D^0}$ shows a characteristic peak, as shown in figure 7. The reconstructed D^{*+} yield is converted into R_c by correcting for the experimental acceptance, decay branching ratios, and hadronisation fraction $P_{c\to D^{*+}}$, and separating the $b\bar{b}$ and $c\bar{c}$ hadronic Z^0 decay components. The requirement of external knowledge of $P_{c\to D^{*+}}$ gives rise to a large systematic error, as discussed above. This method does, however, have the advantages of clean, relatively high statistics signals and well-established experimental techniques. The systematic limitation which comes from needing to know $P_{c\to D^{*+}}B(D^{*+} \to D^0\pi^+)$ can now be reduced using the LEP data themselves using the double-tag technique described next.

With the high statistics LEP-1 data, it is possible to use a more inclusive tag for D^{*+} mesons in a "double-tag" approach. The idea is to look for evidence of D^{*+} decays separately in both thrust hemispheres of the event. The product of hadronisation fractions and branching ratios for $c \to D^{*+} \to \pi^+D^0$ is sufficiently large ($\sim 20\%$) that a statistically useful sample of double-tagged events is available. Two different approaches are in use: the first looks for a fully or partially reconstructed D^0 decay in one hemisphere in conjunction with a further "transition" pion candidate from the $D^{*+} \to D^0\pi^+$ decay, then looks in the opposite hemisphere for a second transition π^+ candidate from the other D^{*-} decay; the second technique simply looks inclusively in the two hemispheres for transition pion candidates. These inclusively identified transition pions can be detected because of the characteristic D^{*+} decay: because the transition π travels close to the original D^{*+} direction. This direction can be approximated fairly well by the axis of the jet containing the transition pion candidate, so that the

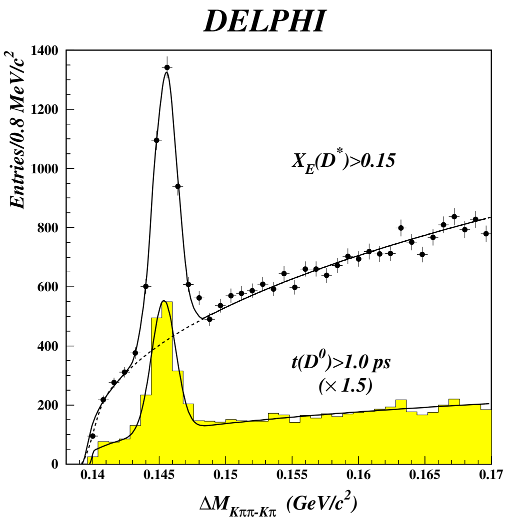

Figure 7: Distribution of reconstructed mass difference $M_{\mathrm{D}^{*+}} - M_{\mathrm{D}^0}$ for $\mathrm{D}^{*+} \rightarrow \mathrm{D}^0\pi^+ \rightarrow \mathrm{K}^-\pi^+\pi^+$ decays as observed by DELPHI.

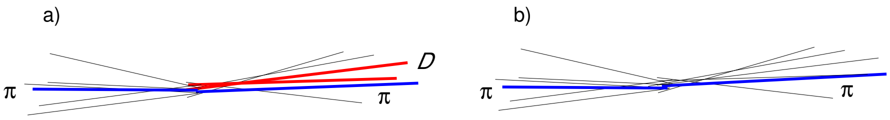

Figure 8: Schematic of D^{*+} double tags: a) inclusive π vs exclusive D^{*+}; b) inclusive π vs inclusive π.

transverse momentum, p_t, of the pion with respect to the jet axis discriminates between the transition pions and other unassociated pions. The two topologies are illustrated in figure 8. The transition pion candidate p_t^2 distributions for the two cases are shown in figure 9. It is evident that there is a large combinatorial background under the transition pion signal, which reduces the statistical power. It can also introduce large systematic uncertainties if the background modelling is incorrect.

As an example of the use of this approach, consider an exclusive tag opposite an inclusive tag. The number of exclusively tagged hemispheres, N_{ex}, and the number of events with both hemispheres tagged, $N_{ex,in}$, in $\mathrm{c\bar{c}}$ events can be written:

$$\begin{aligned} N_{ex} &\propto R_{\mathrm{c}} P_{\mathrm{c}\rightarrow\mathrm{D}^{*+}} B(\mathrm{D}^{*+} \rightarrow \pi\mathrm{D}^0)\varepsilon_{ex} \\ N_{ex,in} &= N_{ex} P_{\mathrm{c}\rightarrow\mathrm{D}^{*+}} B(\mathrm{D}^{*+} \rightarrow \pi\mathrm{D}^0)\varepsilon_{in} \end{aligned}$$

where the efficiencies $\varepsilon_{ex}, \varepsilon_{in}$ for detecting the exclusive and inclusive decays, respectively, are taken from simulation. From these two equations, taking N_{ex} and $N_{ex,in}$ from data, the values of R_{c} and the product $P_{\mathrm{c}\rightarrow\mathrm{D}^{*+}} B(\mathrm{D}^{*+} \rightarrow \pi\mathrm{D}^0)$ can be derived simultaneously, thus giving a "LEP-only" measurement of both. The results obtained for $P_{\mathrm{c}\rightarrow\mathrm{D}^{*+}} B(\mathrm{D}^{*+} \rightarrow \pi\mathrm{D}^0)$ are listed in table 2. The results are seen to be consistent with the lower energy result.

A new type of measurement of R_{c} has recently been developed, initially by OPAL[11]. This technique proceeds by reconstructing at least one decay mode of each main type of weakly decaying charm hadron: D^0,D^+,D_s^+ and Λ_c^+. The known decay branching ratios of these states are combined with detector acceptances to give correction factors from the observed numbers of decays in each mode to the total production rate of the particular hadronic species. Since all produced charmed hadrons

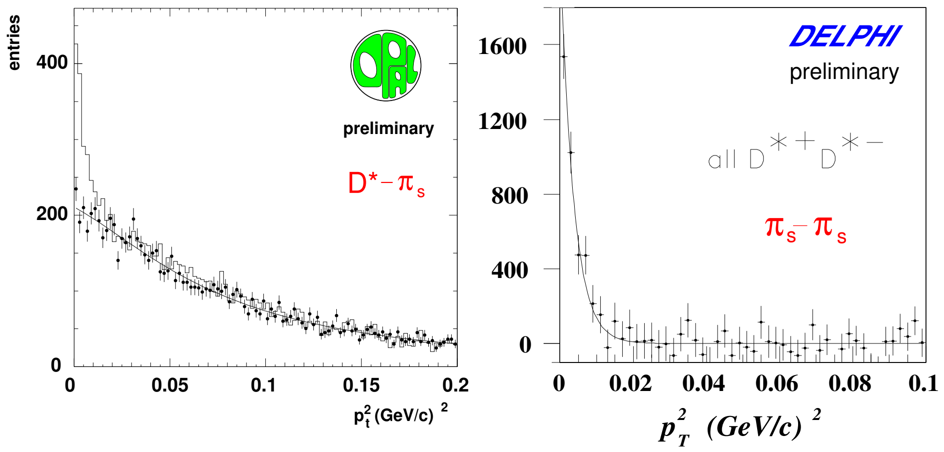

Figure 9: Double D^{*+} tags. The plots show the p_t^2 distributions for transition pion candidates opposite reconstructed D^{*+} mesons in OPAL (left) and opposite transition pion tagged D^{*+}'s in DELPHI (right). Background subtraction has been performed in the right-hand plot.

Table 2: Results for D^{*+} production times decay fraction in $\mathrm{Z}^0 \to \mathrm{c\bar{c}}$ events. For the LEP results the errors are respectively statistical and systematic, for the low energy number these sources have been combined.

	$P_{\mathrm{c}\to\mathrm{D}^{*+}} B(\mathrm{D}^{*+} \to \pi\mathrm{D}^0)$
OPAL (D^{*+}-π)	0.162±0.014±0.013
DELPHI (π-π)	0.166±0.009±0.013
DELPHI (D^{*+}-π)	0.162±0.016±0.019
Lower energy	0.178±0.013

are expected to decay into one of these particles before decaying weakly (except for a small number of charm-strange baryons, for which a small correction is applied), a summation of these numbers gives essentially the entire charm production rate, and thus R_{c}, without needing to put in the hadronisation fractions $P_{c\to\mathrm{X}}$. The assumed completeness of these charmed hadron decays can be written:

$$P_{c\to\mathrm{D}^0} + P_{c\to\mathrm{D}^+} + P_{c\to\mathrm{D_s}^+} + P_{c\to\Lambda_\mathrm{c}} \times (1 + S_{\mathrm{c-baryon}}) = 1$$

where the factor $S_{\mathrm{c-baryon}}$ corrects for the unobserved strange-charm hadron decays. Signals observed in the different channels are illustrated in figure 10. It is evident that this method does not accrue any error from the hadronisation fractions, since they are not required but rather measured directly at the same time as R_{c}. This reduces the systematic error relative to the more traditional single-tag technique. It also allows an independent "LEP-only" check of the energy dependence of the P's measured at the $\Upsilon(4S)$. Experimentally, the reconstruction techniques are also well-established, so that the experimental systematic errors are not large, although the particle identification performance of the detectors remains important. The main limitation of this measurement can, however, be seen in figure 10: the signal to noise ratios are rather poor and the efficiencies are not very high, so that the measurement suffers from quite large statistical errors.

The R_{c} results available are summarised and compared in figure 11. The results have been corrected to the world average value of $B(D^0 \to K\pi)$[10], and the low energy value of $P(\mathrm{c} \to \mathrm{D}^{*+} \to \pi\mathrm{D}^0) = 0.178$, where not measured simultaneously. In addition to the techniques described, results from

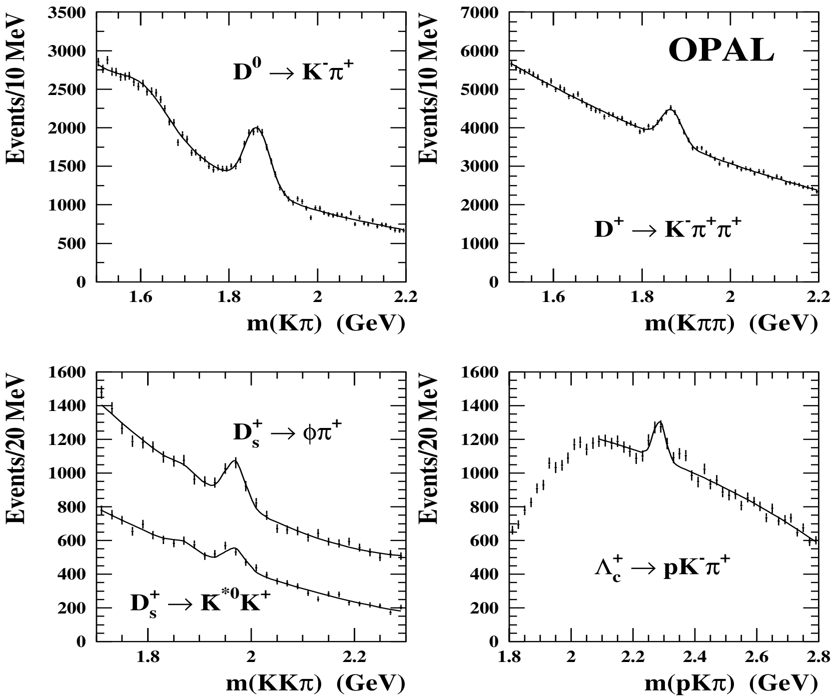

Figure 10: Reconstructed mass distributions in various charm hadron decay channels, from OPAL.

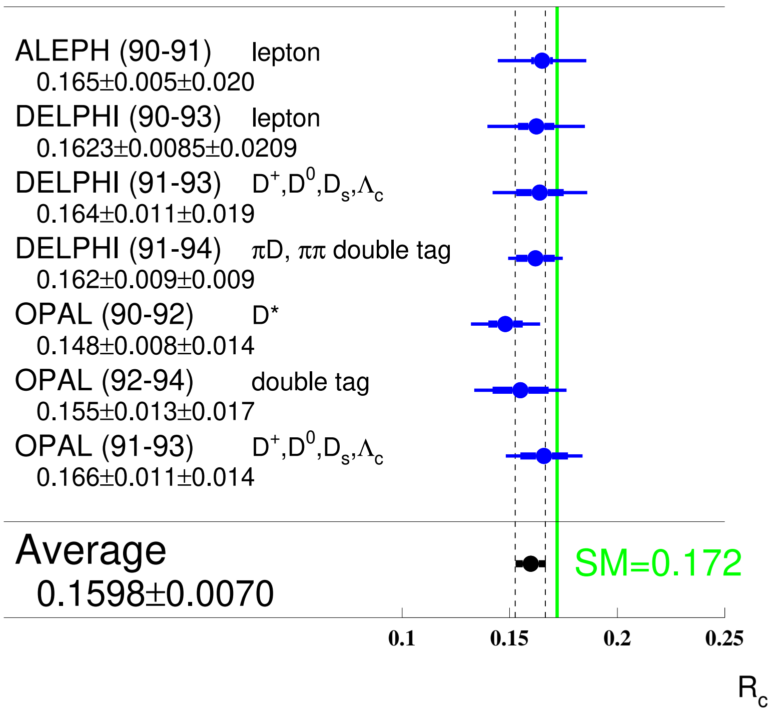

Figure 11: Summary of R_c results. The small γ-Z^0 interference correction (-0.0003) has been applied to the average.

fits to lepton momentum spectra are also shown. The Standard Model expectation is shown as the vertical band. The results are seen to be consistent with each other, and reasonably consistent with the Standard Model expectation. The technique for deriving the average value shown is discussed in section 5.4.

5.2 Measurements of R_{b}

The long lifetimes, and high masses, of b hadrons make it relatively straightforward to isolate large, rather pure, samples of b-tagged events with a lifetime tagging algorithm. Similarly to the case of c tags, systematic uncertainties in b production and decay modelling give rise to large systematic errors on any b tagging efficiency estimated purely from Monte Carlo simulation: indeed the situation is worse than for charm, because much less is known about b decay branching ratios and decay kinematics. This means that "single-tag" measurements, where only one of the b hadrons in an event is tagged, are of relatively little interest for R_{b} measurements because they are systematically limited. As for R_{c}, a solution to this problem lies in the double-tag technique. The high efficiency b tags mean that, in contrast to most R_{c} measurements, the same b tag can be used in both event thrust hemispheres. This leads to a particularly simple formalism for the double-tagging equations, as follows.

The number of tagged hemispheres, N_{t}, can be written as a fraction of the total number of hemispheres, $2N_{\mathrm{had}}$ (twice the number of hadronic events):

$$\frac{N_{\mathrm{t}}}{2N_{\mathrm{had}}} = \varepsilon^{\mathrm{b}} R_{\mathrm{b}} + \varepsilon^{\mathrm{c}} R_{\mathrm{c}} + \varepsilon^{\mathrm{uds}}(1 - R_{\mathrm{b}} - R_{\mathrm{c}}) \tag{1}$$

where ε^{b},ε^{c}, and $\varepsilon^{\mathrm{uds}}$ are the efficiencies for tagging a hemisphere in $\mathrm{b\overline{b}}$, $\mathrm{c\overline{c}}$ and light quark events. The number of events in which both hemispheres are tagged, N_{tt}, can similarly be written:

$$\frac{N_{\mathrm{tt}}}{N_{\mathrm{had}}} = C_{\mathrm{b}}(\varepsilon^{\mathrm{b}})^2 R_{\mathrm{b}} + (\varepsilon^{\mathrm{c}})^2 R_{\mathrm{c}} + (\varepsilon^{\mathrm{uds}})^2(1 - R_{\mathrm{b}} - R_{\mathrm{c}}) \tag{2}$$

Although the same tag is employed in the two event hemispheres, the efficiency to tag the second hemisphere can differ slightly from that to tag the first, because of tagging efficiency correlations. These correlations are only important for $\mathrm{b\overline{b}}$ events, and they lead to the introduction of the correlation factor C_{b}, which is approximately unity.

There are two qualitatively different types of b lifetime tag in use for R_{b} measurements. The first, originated by ALEPH[12] and also employed by DELPHI, uses a compound probability derived from the significance of impact parameters of tracks in the event hemisphere. The second, employed by OPAL[13] and SLD[14] in different variants, relies on the reconstruction of a secondary vertex in each event hemisphere, and uses the separation of the secondary vertex from the primary event vertex to distinguish b events from lighter flavours. In addition, SLD also find the invariant mass of the tracks assigned to the vertex (adding an estimate of the neutrino momentum) provides substantial discriminating power between charm and bottom hadron decays. The overall performance of these tags is to give hemisphere b tagging efficiencies of 20-40%, with a b purity of the tagged hemispheres of 92-98%.

Equations 1 and 2 can be solved simultaneously for ε^{b} and R_{b}, if C_{b}, ε^{c}, $\varepsilon^{\mathrm{uds}}$ and R_{c} are known. These latter parameters have to be derived from external information and Monte Carlo modelling, but the uncertainties on them lead to much reduced systematic uncertainties on R_{b} than would be obtained from the pure single tag approach. The disadvantage of the double tag technique is that the statistical error on R_{b} is greatly increased over that from a single tag, since it is dominated by the number of double-tagged events. The high performance of modern lifetime tags, and the huge LEP-1 data statistics, mean that this is not a debilitating limitation, however. The challenge of the R_{b} measurement with the double-tag technique thus reduces to how well C_{b} and ε^{c} (and the rather smaller $\varepsilon^{\mathrm{uds}}$) can be determined, keeping in mind that ε^{b} must be kept high enough that the double tag statistics do not become a problem.

The main sources of uncertainty on ε^{c} come from the c hadronisation fractions in Z^0 decays, and the knowledge of the decay multiplicity distributions for different c hadrons. The hadronisation fractions are important for ε^{c} because of the very different lifetimes of the different c hadron species, which means they have very different probabilities to be mistagged as b hadrons. As discussed above in section 5.1, these hadronisation fractions had, until recently, to be taken from measurements at lower energies, principally around the $\Upsilon(4S)$. Now, however, they have been measured directly at LEP, and the values observed are found to be in good agreement with the low energy extrapolations. The inclusive charged particle decay multiplicity distributions have been measured[15] by Mark-III for D^+, D^0 and D_s^+, and these results are used directly in deriving ε^{c}. The shapes of these distributions are important because high multiplicity c hadron decays (particularly those of the longer living D^+) are most likely to be mistagged as b decays, and thus contribute most to ε^{c}. The errors arising from the knowledge of charm hadron lifetimes, and charm fragmentation, are less important in this measurement.

Correlations in the tagging efficiencies in the two hemispheres are introduced by three principal effects: gluon radiation; non-uniform detector acceptance; and the primary vertex information, which is shared between the two hemispheres. The first and third of these effects are potentially most hazardous, the second can be well understood using single-tagging rates observed in the data.

Gluon radiation gives rise to hemisphere efficiency correlations of two different classes: firstly, radiation of a sufficiently hard gluon can mean that the primary b and $\overline{\mathrm{b}}$ quarks recoil into the same event thrust hemisphere; and secondly softer gluon radiation introduces a correlation of the b and $\overline{\mathrm{b}}$ momenta. The first effect gives a negative efficiency correlation, pulling C_{b} below unity, the second effect tends to produce a positive efficiency correlation, because both b and $\overline{\mathrm{b}}$ momenta tend to be lowered together by gluon emission, and the tagging efficiency rises with b momentum. There can be other, smaller, effects related to gluon emission in addition to this correlation through the magnitude of the momentum of the b in the same hemisphere as the tag. These effects have to be estimated using Monte Carlo. Checks with data of the correct simulation of these correlating effects can be made, but there remains some residual reliance on a reasonably correct Monte Carlo simulation.

The knowledge of the primary vertex can introduce an efficiency correlation in two ways: if the primary vertex *position* is mis-estimated, this can give a tagging efficiency correlation; or if the *error* on the primary vertex position is mis-estimated, this can also give an efficiency correlation since it is normal to make requirements on the significance of lifetime information (i.e. normalised by the error) when constructing the b tag. These correlations can be estimated using Monte Carlo, varying the vertex position and the error within their uncertainties.

Overall, the main source of uncertainty on C_{b} comes from gluon radiation, since it is most difficult to understand comprehensively. The area of hemisphere correlations is under intense study within the LEP experiments. The size of hemisphere correlations, expressed both in terms of C_{b} and the alternative variable $\lambda_{\mathrm{b}} \equiv (C_{\mathrm{b}}-1)\varepsilon^{\mathrm{b}}/(1-\varepsilon^{\mathrm{b}})$, are shown in table 3. It is noticeable that the correlations of the vertex tag measurements, from OPAL and SLD, are significantly smaller than those of the impact parameter probability tags, as used by ALEPH and DELPHI. This seems to be at least partly related to the different use of primary vertex information in the different tag types.

The R_{b} results[16] available are shown in figure 12. In some cases small corrections have been applied to the results for consistency with the LEP electroweak heavy flavour working group recommendations. The Standard Model expectation is shown as the vertical band. The results are seen to be consistent with each other. The technique for deriving the average value shown is discussed in section 5.4. The average value is seen to be slightly higher than the Standard Model prediction.

5.3 Heavy Flavour Asymmetries

Forward-backward asymmetry measurements have been made for Z^0 decays to heavy quarks. For b quarks lifetime and lepton tags are both important for asymmetry measurements: the lower efficiency of the lepton tags is compensated by the direct information the lepton charge gives on the decaying b

Table 3: Hemisphere tagging efficiency correlations.

	C_b	λ_b	ε^b	$C_b - 1$
OPAL (92–94)	1.006 ± 0.003		23%	$+0.6 \pm 0.3\%$
ALEPH (92)		$-2.0 \pm 0.3\%$	26%	$-5.7 \pm 0.8\%$
DELPHI (91)		$-0.1 \pm 0.4\%$	24%	$-0.4 \pm 1.3\%$
DELPHI (92)		$-0.3 \pm 0.2\%$	20%	$-1.0 \pm 0.7\%$
DELPHI (93)		$-1.3 \pm 0.2\%$	21%	$-4.8 \pm 0.6\%$
SLD (93–95)		$+0.5 \pm 0.2\%$	36%	$-0.9 \pm 0.4\%$

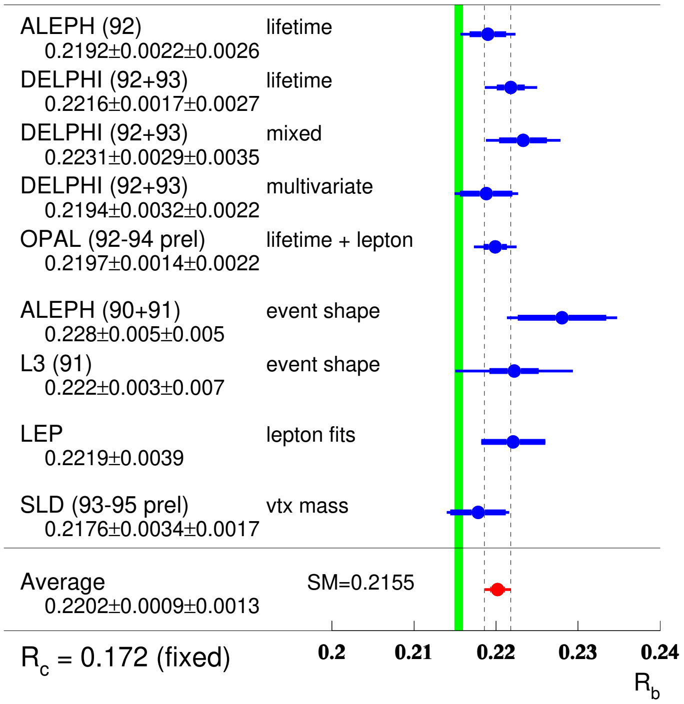

Figure 12: R_b results. The small $\gamma - Z$ interference correction ($+0.0003$) has been applied to the average.

quark charge. For lifetime tagged asymmetry measurements the b quark charge must be inferred from a jet-charge measure, which introduces a significant statistical penalty. For c quarks reconstructed particle tags give the decaying c quark charge directly. Lepton tags are also useful for c asymmetries, but in this case the need to separate the different sources of leptons introduces a statistical penalty, so that eventually lepton and reconstructed particle tags give similar c asymmetry precisions. The results are summarised in figures 13 and 14. Good consistency with the Standard Model expectations are found.

In addition to these forward-backward asymmetry measurements at LEP, SLD have also measured the polarised left-right forward-backward asymmetries for heavy quarks. The results obtained are included in the next section.

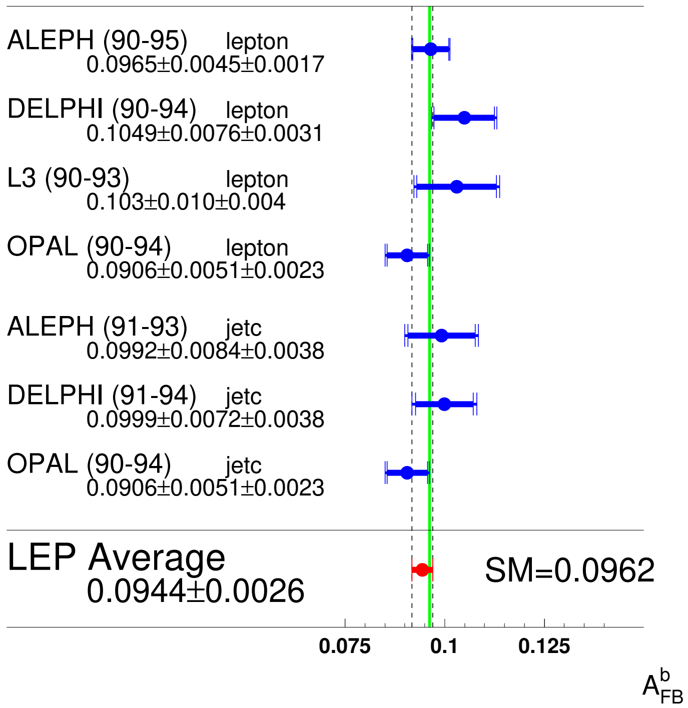

Figure 13: $A^{\mathrm{b}}_{\mathrm{FB}}$ results. Both lepton fit, "lepton", and lifetime tag plus jet-charge identification, "jetc", approaches are used.

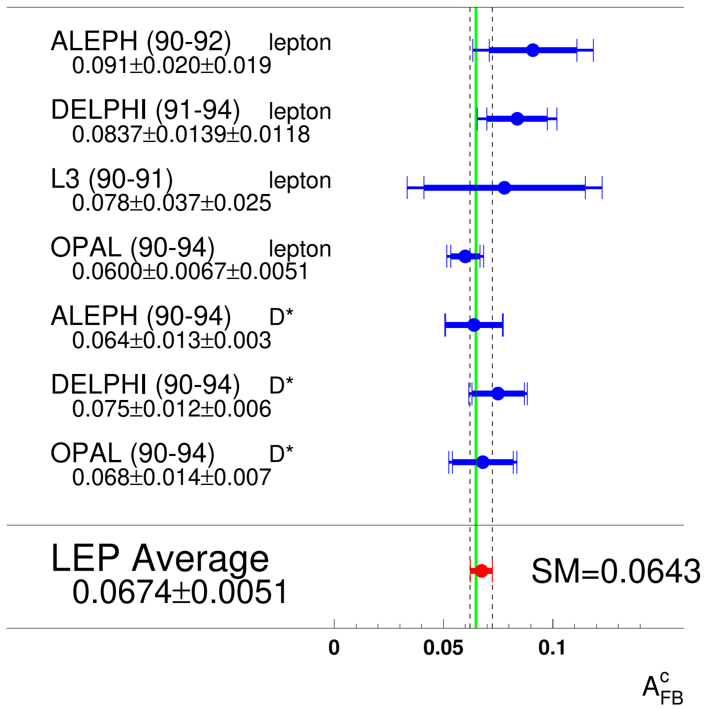

Figure 14: $A^{\mathrm{c}}_{\mathrm{FB}}$ results. The two types of measurements are denoted "lepton" for lepton tags, "D*" for reconstructed D^{*+} tags.

5.4 Combining Heavy Flavour Electroweak Results

A variety of electroweak measurements in the heavy quark sector have been summarised above. Many of the analyses measure more than one electroweak observable, or depend on some other external parameter: for example, asymmetry measurements typically measure both $A_{\mathrm{FB}}^{\mathrm{b}}$ and $A_{\mathrm{FB}}^{\mathrm{c}}$, and R_{b} measured via a double-tag depends on the assumed value of R_{c}. In addition, there are sizeable correlated systematic uncertainties between measurements, both of the same and different electroweak observables, within and between experiments. A correct and consistent averaging of all these results is thus not completely straightforward, as all these correlated effects should be taken into account. This is achieved in the framework of the LEP electroweak heavy flavour group averaging program[17], which handles all these interdependences consistently. Ranges for the variation of common systematic error sources are also agreed by the LEP experiments, to allow a consistent combination. The procedure constructs a covariance matrix between all the different electroweak measurements, and a chi-squared minimisation is used to extract the average heavy flavour electroweak quantities. The procedure has been checked extensively with simpler averages. It has also been verified that changes in error correlation assumptions between different measurements are unimportant, for cases where the level of correlation of a specific correlated error source is unclear.

The results obtained by combining the LEP and SLD heavy flavour measurements via this procedure are[16]:

$$\begin{aligned}
R_{\mathrm{b}} &= 0.2211 \pm 0.0016 \\
R_{\mathrm{c}} &= 0.1598 \pm 0.0070 \\
A_{\mathrm{FB}}^{0,\mathrm{b}} &= (10.00 \pm 0.28)\% \\
A_{\mathrm{FB}}^{0,\mathrm{c}} &= (7.59 \pm 0.51)\% \\
\mathcal{A}_{\mathrm{b}} &= 0.842 \pm 0.053 \\
\mathcal{A}_{\mathrm{c}} &= 0.618 \pm 0.090 \\
\mathrm{Br}(\mathrm{b} \rightarrow \ell) &= (11.12 \pm 0.23)\% \\
\mathrm{Br}(\mathrm{b} \rightarrow \mathrm{c} \rightarrow \ell^{+}) &= (7.81 \pm 0.42)\% \\
\overline{\chi} &= 0.1221 \pm 0.0052 \\
P(\mathrm{c} \rightarrow \mathrm{D}^{*+} \rightarrow \pi \mathrm{D}^{0}) &= 0.168 \pm 0.007
\end{aligned}$$

Note that the $\mathcal{A}_{\mathrm{b}}$ and $\mathcal{A}_{\mathrm{c}}$ results quoted here come solely from the polarised asymmetries measured at SLD. LEP measurements dominate the other results. The overall χ^2 per degree of freedom for this fit is $40.8/(76-10)$. The measured value of R_{b} is found to be quite strongly dependent on the value of R_{c} obtained, with a correlation coefficient between the two averaged results of -30%. It is therefore also instructive to repeat the fit fixing R_{c} to its Standard Model value of 0.172. This gives $R_{\mathrm{b}}(R_{\mathrm{c}} = 0.172) = 0.2202 \pm 0.0016$. This result is compared with the Standard Model expectation in figure 15. The correlation between the R_{b} and R_{c} results is illustrated in figure 16. It can be seen that the average R_{c} lies a little below the Standard Model expectation, and the average R_{b} somewhat above. The difference in the χ^2 of the combined fit between these central values and the Standard Model expectation (for a top quark mass of 175 GeV) is 10.3. What, if any, conclusions may be drawn from this intriguing apparent discrepancy must await finalised analyses on the full LEP-1, and SLD, data samples[4].

[4] At the 1996 summer conferences, several new preliminary results on these heavy quark electroweak measurements were available. In particular, new precise R_{b} results were reported from ALEPH and SLD, using sophisticated new tagging algorithms. In the case of ALEPH a completely new multiple tag technique has been developed. With the inclusion of these new results, the combined central values of R_{b} and R_{c} from the consistent fit become $R_{\mathrm{b}} = 0.2179 \pm 0.0012$, $R_{\mathrm{c}} = 0.1715 \pm 0.0056$, significantly closer to the Standard Model expectations.

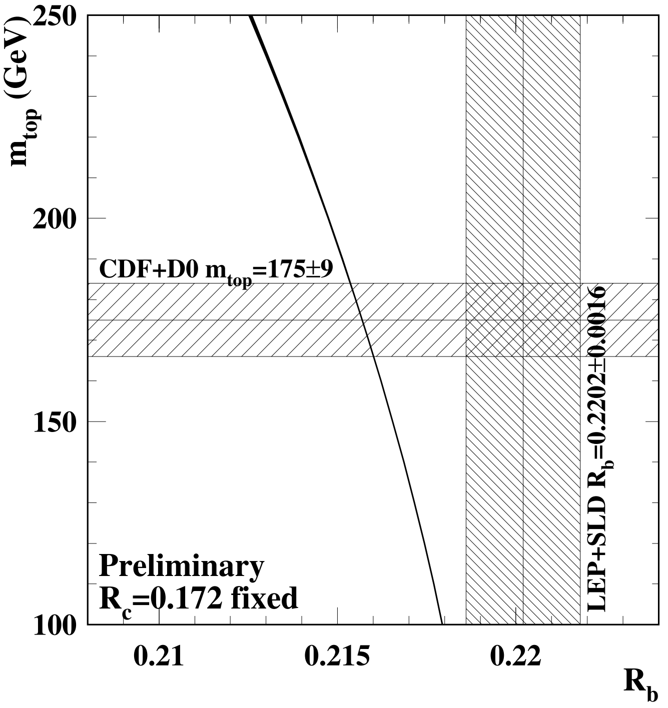

Figure 15: The world average values for R_b with R_c fixed to its Standard Model expectation, compared to the Standard Model prediction for different top mass values. The top mass measured directly at the Tevatron is shown for comparison.

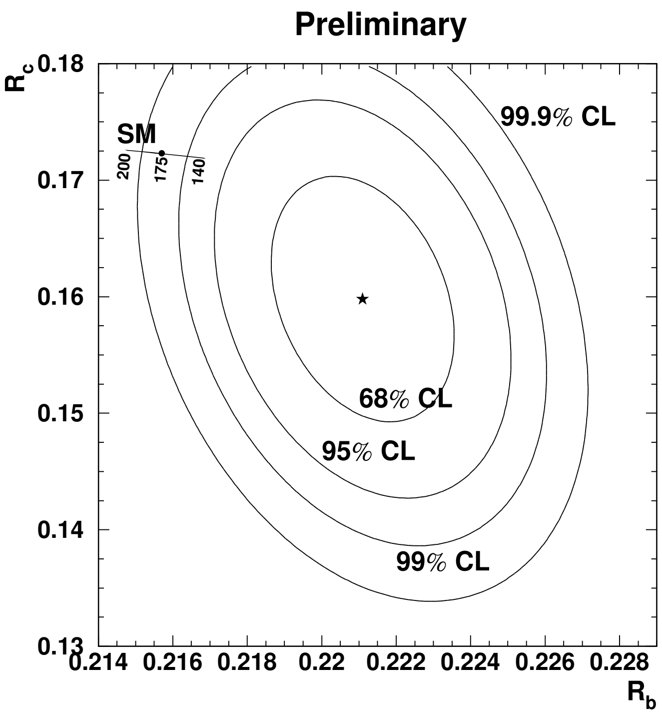

Figure 16: The world average values for R_c and R_b with various confidence level error contours. The Standard Model expectation is also shown for the range of top masses indicated.

Table 4: Summary of Electroweak Measurements. The "SM fit" numbers come from a Standard Model fit to all data, taking a fixed $m_{\mathrm{H}} = 300$ GeV.

	Measurement	SM Fit	Pull
LEP			
line-shape/lepton asy			
M_{Z} [GeV]	91.1884 ± 0.0022	91.1869	0.7
Γ_{Z} [GeV]	2.4964 ± 0.0032	2.4979	-0.5
$\sigma_{\mathrm{had}}^{\mathrm{pole}}$ [nb]	41.490 ± 0.078	41.454	0.5
R_{ℓ}	20.788 ± 0.032	20.770	0.6
$A_{\mathrm{FB}}^{0,\ell}$	0.0171 ± 0.0011	0.0159	1.1
τ polarization:			
$\mathcal{A}_{\tau}$	0.1394 ± 0.0069	0.1455	-0.9
$\mathcal{A}_{\mathrm{e}}$	0.1429 ± 0.0079	0.1455	-0.3
b and c quark results:			
R_{b}	0.2215 ± 0.0017	0.2155	3.5
R_{c}	0.1596 ± 0.0070	0.1725	-1.8
$A_{\mathrm{FB}}^{0,\mathrm{b}}$	0.1002 ± 0.0028	0.1020	-0.6
$A_{\mathrm{FB}}^{0,\mathrm{c}}$	0.0756 ± 0.0051	0.0728	0.5
$\mathrm{q\overline{q}}$ charge asymmetry:			
$\sin^2\theta_{\mathrm{W}}^{\mathrm{eff},\ell}$	0.2320 ± 0.0010	0.23171	0.3
SLD			
$\sin^2\theta_{\mathrm{W}}^{\mathrm{eff},\ell}$ (A_{LR})	0.23049 ± 0.00050	0.23172	-2.4
R_{b}	0.2176 ± 0.0039	0.2155	0.5
$\mathcal{A}_{\mathrm{b}}$	0.842 ± 0.052	0.934	-1.8
$\mathcal{A}_{\mathrm{c}}$	0.618 ± 0.091	0.667	-0.5
$\mathrm{p\overline{p}}$ and νN			
M_{W} [GeV] ($\mathrm{p\overline{p}}$)	80.33 ± 0.15	80.37	-0.2
$\sin^2\theta_{\mathrm{W}}$ (νN)	0.2257 ± 0.0047	0.2232	0.5

6 Combined Electroweak Fits

The diverse measurements of different Standard Model parameters described in the preceding sections can be consistently compared with Standard Model expectations in the framework of a combined electroweak fit. If the Standard Model structure for radiative corrections is assumed, the measurements can be used to infer information about the top quark and Higgs boson masses. Use, in addition, of the direct measurement of the top mass from the Tevatron allows better constraints to be placed on the Higgs boson mass. Since these model fits make use of leading orders of electroweak radiative corrections to derive these unknown parameters, it is essential that the theoretical precision of these predicted corrections be known. This issue has been addressed recently[18], where it was concluded that these theoretical uncertainties are still sufficiently well understood, after a detailed comparison of different electroweak fitting program codes. In contrast another important input for these fits, the value of the fine structure constant, $\alpha(M_{\mathrm{Z}})$, at the Z^0 pole, is known with a relatively limited precision, coming from the limited experimental knowledge of the total cross-section for $\mathrm{e^+e^-}$ annihilation at low energies. For the fits, the value $\alpha(M_{\mathrm{Z}}) = 1/(128.896 \pm 0.090)$ is used. This uncertainty translates to an error on $\sin^2\theta_{\mathrm{W}}^{\mathrm{eff},\ell}$ of 0.00023. This is not much smaller than the experimental error from LEP and SLD.

The consistency of the individual measurements to the results of such a consistent fit to all the LEP electroweak data is shown in table 4. All results are in reasonable agreement with expectation, except for R_{b}, which contributes a pull of 3.5[5].

[5] At the 1996 summer conferences, the results and corresponding pulls had changed somewhat with the addition of

Table 5: Electroweak fit results. The first error shown is experimental, the second shows the effect of varying m_{H} from the central value assumed of 300 GeV to 60 and 1000 GeV.

	LEP	LEP + SLD
m_{top} [GeV]	$172\,^{+9}_{-10}\,^{+18}_{-20}$	$180\,^{+8}_{-9}\,^{+18}_{-21}$
$\alpha_s(M_{\mathrm{Z}})$	$0.124 \pm 0.004\ \pm 0.002$	$0.123 \pm 0.004\ \pm 0.002$
χ^2/d.o.f.	15/9	24/12

	LEP + SLD + $\mathrm{p\overline{p}}$ and νN data
m_{top} [GeV]	$179 \pm 8\ ^{+18}_{-20}$
$\alpha_s(M_{\mathrm{Z}})$	$0.123 \pm 0.004\ \pm 0.002$
χ^2/d.o.f.	25/14

These fits can be repeated with different inputs: either purely LEP electroweak data, or combining LEP and SLD, or combining also with the W mass measurement from $\mathrm{p\overline{p}}$ colliders and using $\sin^2\theta_{\mathrm{W}}$ from neutrino-nucleon scattering. Table 5 shows examples, for the case where $\alpha_s(M_{\mathrm{Z}})$ is left free. The value of $\alpha_s(M_{\mathrm{Z}})$ extracted can be compared with the value from hadronic event shape measurements of $\alpha_s(M_{\mathrm{Z}}) = 0.123 \pm 0.006$. R_{b} and R_{c} contribute about 12 to the fit χ^2.

When the directly measured top mass, 175±9 GeV, from $\mathrm{b\overline{b}}$ experiments is included as an external constraint in the fits, there is some sensitivity of the results to the Higgs boson mass, as shown in figure 17. However the precision is rather limited, and somewhat sensitive to the variables included in the fit. About the best that can be said at present is that within the framework of the Standard Model, the data seem to favour a Higgs boson mass in the lower regions of the experimentally and theoretically allowed range between 60 and 1000 GeV.

7 The LEP Energy Upgrade

The first step of the energy upgrade of LEP was taken in the autumn of 1995, towards the LEP-2 programme of 1996-1999. The main aim of this running period was to learn about the operation of superconducting radio-frequency cavities at high energy, essential for the success of LEP-2 in the next few years. In addition, a physics goal of this run had been set to try to accumulate 5 pb^{-1} of data at high energies. In the event this goal was reached, with 6 pb^{-1} being collected by all four experiments, 3 pb^{-1} each at the two centre-of-mass energies of 130 and 136 GeV. In addition a tiny amount of data (50 nb^{-1}) was collected at 140 GeV.

These data were sufficient to study the main features of fermion pair production at energies above the Z^0: namely that in addition to events where the fermion pair carries close to the full centre-of-mass energy, a large number of events were also seen where the fermion-pair effective centre-of-mass energy was close to the Z^0, after hard initial-state photon radiation – the so-called "radiative return". The characteristics of the full energy non-radiative events are of most interest, since they reflect the new high energy. Measurements[19] have been made of the total and non-radiative cross-sections (see figure 18) and forward-backward asymmetries, as well as studies of QCD observables leading to measurements[20] of α_s at these energies.

In a purely Standard Model framework, these high energy data provide little extra information about the theory. Nonetheless it is interesting to incorporate them into a more general fit framework, to assess their consistency with the Standard Model. This has been done in the formalism of the

new measurements. Specifically, the R_{b} pull decreased to 1.8, and those from A_{LR} and $A_{\mathrm{FB}}^{0,\mathrm{b}}$ changed to -2.2 and -1.8, respectively.

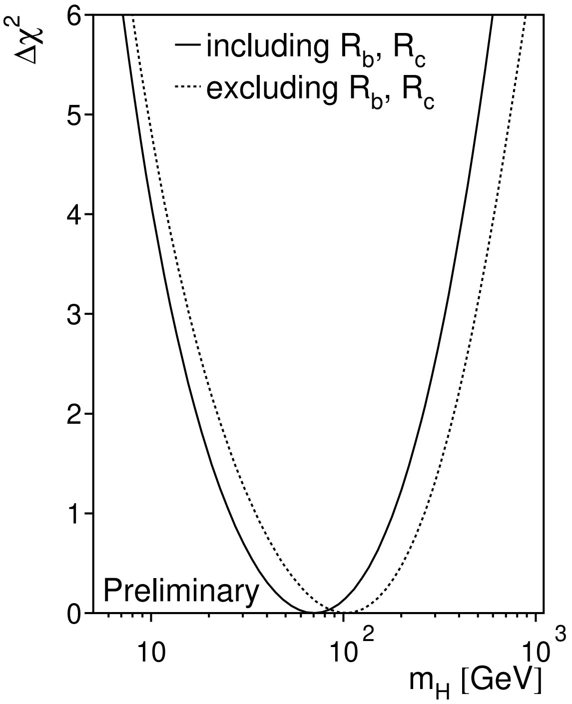

Figure 17: χ^2 variation from the Standard Model fit as m_{H} varies. The full curve shows the combined fit of all LEP results, the dashed curve excludes R_{b} and R_{c}, to show the sensitivity to those inputs.

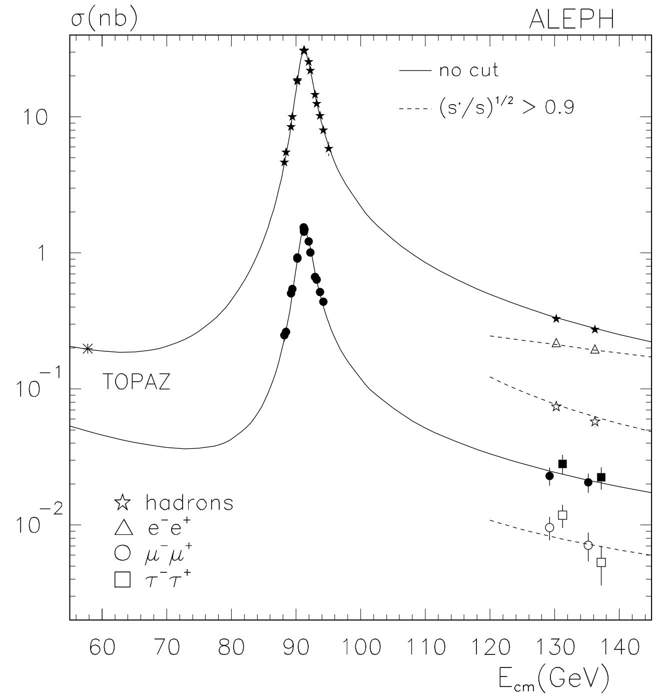

Figure 18: Fermion-pair cross-sections at and above the Z^0, from ALEPH. Total (solid symbol) and non-radiative (open symbol) cases are shown.

"S-matrix" fit to the Z^0 lineshape, where to lowest-order the $q\bar{q}$ cross-section is written:

$$\sigma_{q\bar{q}}(\sqrt{s}) = \frac{A_\gamma}{s} + \frac{A_{\gamma Z^0}(s - M_Z^2) + A_{Z^0}\, s}{(s - M_Z^2)^2 + s^2\Gamma_Z^2/M_Z^2}$$

with the A's parameters to be fit. In Standard Model fits, the relative sizes of A_γ, $A_{\gamma Z^0}$ and A_{Z^0} are fixed, so that M_Z and Γ_Z are extracted. In the "S-Matrix" fit $A_{\gamma Z^0}$ can float, in which case the M_Z precision is reduced. The 130-136 GeV data are particularly sensitive to this interference term, which is also commonly expressed as a parameter j_{had} (closely related to $A_{\gamma Z^0}$, and taking value 0.22 in the Standard Model). Error ellipses for j_{had} vs. M_Z from the S-matrix fits are illustrated in figure 19.

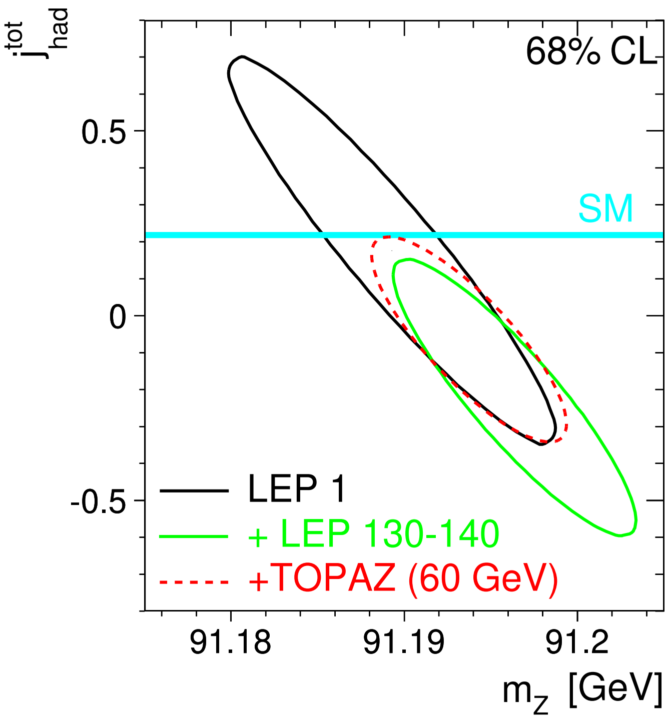

Figure 19: j_{had} vs. M_Z resulting from S-matrix fits to LEP-1, LEP-1 plus 130-140 GeV data, and including also a measurement from TOPAZ. The Standard Model expectation $j_{\mathrm{had}} = 0.22$ is shown by the horizontal line.

8 LEP-2 and the W Mass Measurement

The LEP-2 programme itself begins in the summer of 1996, albeit with relatively short test runs primarily to check the operation of the machine. A centre-of-mass energy of 161 GeV is available in June-August 1996, and 172 GeV in the autumn. In both cases luminosities of approximately 10 pb^{-1} should be accumulated – lower than normal for a year of LEP-2 operation because of the continuing cavity installation programme, and the need to learn how to operate the accelerator well at the new high energies. During the subsequent three years of LEP-2 data-taking, a total integrated luminosity of 500 pb^{-1} per experiment is anticipated, mostly collected at 188-192 GeV centre-of-mass energy.

The main electroweak precision measurement to be made at LEP-2 is the measurement of the mass of the W boson, complementing the LEP-1 Z^0 studies. Two very different types of measurements are possible at LEP-2 energies, but with similar precision per unit integrated luminosity collected. The first technique relies on measuring the W-pair production cross-section just above the threshold, at approximately 161 GeV. The second technique uses direct reconstruction of the W decay products, together with an energy-momentum constraint from the known beam energies. This method only has a competitive statistical precision for beam energies above about 170 GeV, because below that the W-pair cross-section is too low.

These two approaches have different advantages and disadvantages, which are reflected in different expected experimental systematic errors. In particular, it is not yet known whether the channel where both W's decay hadronically can be used for the direct reconstruction technique, or whether interconnection effects between the two hadronic systems produced by the two W's will give rise to unmeasurable systematic shifts in the reconstructed W mass. This effect should not be significant for cases where one W decays hadronically and the other leptonically, however, which is just as important a decay channel for the direct reconstruction technique. It can be hoped, nonetheless, that the W mass measurement at LEP-2 will remain statistics limited with the integrated luminosity anticipated, even when combining the results from the four experiments. As at LEP-1, one of the main potential sources of systematic error for the boson mass measurement will be the knowledge of the beam energy. This error source is correlated between both measurement methods, and the experiments, so is particularly important to understand well.

Overall, the expected W mass precision from LEP-2 data-taking, assuming 500 pb^{-1} per experiment, and combining all four experiments, is 30-40 MeV. This compares with the currently published measurements from $\mathrm{p\overline{p}}$ colliders [21], which have a combined precision of 125 MeV. Already from the first short 161 GeV data-taking run, with 10 pb^{-1} per experiment, a combined LEP W mass error of approximately 200 MeV should be achieved[6]. A similar precision may be attainable from the 1996 172 GeV data-taking. Ultimately, after the main injector upgrade of the Tevatron, the CDF and D0 experiments hope to have a final W mass precision comparable to that from the full LEP-2 programme, a few years later. These measurements will probe M_{W} to the same level of precision that it is currently predicted by the Standard Model electroweak fits – and thus will provide a further crucial precise Standard Model test.

9 Summary and Conclusions

In summary, the LEP-1 programme has provided an impressive range of high precision electroweak results, and will continue to do so for some more time as the analysis of the full data sample is completed. The measurements are nicely complemented by those at the SLC using a polarised electron beam. Overall, the agreement with the Standard Model of all these measurements is good. Recently apparent discrepancies have been reported in the Standard Model description of the measured values of R_{b} and R_{c} – the latter discrepancy is now reduced, however, and the former remains at the level of 3 standard deviations: insufficient to claim any significant evidence for a breakdown of the Standard Model, particularly when the excellent agreement of most of the rest of the electroweak predictions with measurement is considered.

Looking to the future, the energy upgrade of LEP has produced its first results, and the LEP-2 programme is now just starting. The outlook for the next couple of years is therefore bright, with the completion of LEP-1 analyses, and the first precise results from LEP-2.

Acknowledgments

I wish to thank the organisers, and particularly Professor O.Nachtmann, for their invitation to attend this workshop. I would also like to thank M.D.Hildreth and P.S.Wells for their help preparing the talk.

[6] Preliminary results from the 161 GeV data-taking were presented at CERN in October 1996. A preliminary combined W mass measurement from the 161 GeV data of 80.4±0.2±0.1 GeV was presented [22].

References

[1] *Physics at LEP-1*, eds. J.Ellis and R.Peccei, CERN 86-02.

[2] The LEP Collaborations, ALEPH, DELPHI, L3 and OPAL, the LEP Electroweak Working Group and the SLD Heavy Flavor Group, CERN-PPE/96-183.

[3] R. Assman *et al.*, *Z. Phys.* C **66**, 567 (1995).

[4] G. Wilkinson, talk presented at ICHEP96, Warsaw, 25-31 July 1996, to appear in the proceedings.

[5] See reference 2., or for an earlier summary:
The LEP Collaborations, ALEPH, DELPHI, L3, OPAL and the LEP Electroweak Working Group, CERN-PPE/95-172.

[6] SLD Collab., K. Abe *et al.*, *Phys. Rev. Lett.* **73**, 25 (1994);
M. Woods, in *Proceedings of the International Europhysics Conference on High Energy Physics*, ed. J. Lemonne, C. Vander Velde, F. Verbeure (World Scientific, Singapore, 1996).

[7] L. Malgeri, talk presented at the XXXI Rencontres de Moriond, March 1996.

[8] See, for example: T. Behnke and D.G. Charlton, *Physica Scripta* **52**, 133 (1995).

[9] See, for example: P. Bamert *et al.*, *Phys. Rev.* D **54**, 4275 (1996), and references therein.

[10] Particle Data Group, L. Montanet *et al.*, *Phys. Rev.* D **50**, 1 (1994); and 1995 partial update.

[11] OPAL Collab., G. Alexander *et al.*., *Z. Phys.* C **72**, 1 (1996).

[12] ALEPH Collab., D. Buskulic *et al.*, *Phys. Lett.* B **313**, 535 (1993).

[13] OPAL Collab., R. Akers *et al.*, *Z. Phys.* C **65**, 17 (1995).

[14] E. Etzion, talk presented at the XXXI Rencontres de Moriond, March 1996.

[15] MARK III Collab., D. Coffman *et al.*, *Phys. Lett.* B **263**, 135 (1991).

[16] M.D. Hildreth, talk presented at the XXXI Rencontres de Moriond, March 1996.

[17] The LEP Experiments: ALEPH, DELPHI, L3 and OPAL, *Nucl. Instrum. Methods* **A378**, 101 (1996).

[18] *Reports of the working group on precision calculations for the* Z^0 *resonance*, eds. D. Bardin, W. Hollik and G. Passarino, CERN 95-03.

[19] L3 Collab., M. Acciarri *et al.*, *Phys. Lett.* B **370**, 195 (1996);
OPAL Collab., G. Alexander *et al.*, *Phys. Lett.* B **376**, 232 (1996);
ALEPH Collab., D. Buskulic *et al.*, *Phys. Lett.* B **378**, 373 (1996).

[20] L3 Collab., M. Acciarri *et al.*, *Phys. Lett.* B **371**, 137 (1996);
OPAL Collab., G. Alexander *et al.*, *Z. Phys.* C **72**, 191 (1996);
ALEPH Collab., D. Buskulic *et al.*, CERN-PPE/96-043;
DELPHI Collab., P. Abreu *et al.*, CERN-PPE/96-130.

[21] CDF Collab., F. Abe *et al.*, *Phys. Rev. Lett.* **75**, 11 (1995), *Phys. Rev.* D **52**, 4784 (1995);
CDF Collab., F. Abe *et al.*, *Phys. Rev. Lett.* **65**, 1990 (2243), *Phys. Rev.* D **43**, 2070 (1991);
D0 Collab., S. Abachi *et al.*, *Phys. Rev. Lett.* **77**, 3309 (1996);
UA1 Collab., C. Albajar *et al.*, *Z. Phys.* C **44**, 15 (1989);
UA2 Collab., J. Alitti *et al.*, *Phys. Lett.* B **276**, 354 (1992).

[22] N.Watson, CERN Particle Physics Seminar, 8 October 1996; see also
OPAL Collab., K. Ackerstaff *et al.*, CERN-PPE/96-141, to appear in *Phys. Lett.* B.